Published in final edited form as:
Eur J Oral Sci. 2011 December ; 119(Suppl 1): 97–102. doi:10.1111/j.1600-0722.2011.00900.x.

Effect of phosphorylation on the interaction of calcium with leucine-rich amelogenin peptide

Elvire Le Norcy[a,,b], **Seo-Young Kwak**[a,,b], **Marc Allaire**[c], **Peter Fratzl**[d], **Yasuo Yamakoshi**[e], **James P. Simmer**[e], and **Henry C. Margolis**[a,,b,*]

[a]Department of Biomineralization, The Forsyth Institute, Cambridge, MA, USA.

[b]Department of Developmental Biology, Harvard School of Dental Medicine, Boston, MA, USA.

[c]National Synchrotron Light Source, Brookhaven National Laboratory, Upton, NY, USA.

[d]Department of Biomaterials, Max Planck Institute of Colloids and Interfaces, Research Campus Golm, D-14424 Potsdam, Germany

[e]Department of Biologic and Materials Sciences, University of Michigan School of Dentistry, Ann Arbor, MI, USA.

Abstract

Amelogenin undergoes self-assembly and plays an essential role in guiding enamel mineral formation. The Leucine-Rich Amelogenin Peptide (LRAP) is an alternative splice product of the amelogenin gene composed of the N-terminus (containing the only phosphate group) and C-terminus of full-length amelogenin. This study was conducted to further investigate the role of phosphorylation in LRAP self-assembly in the presence and absence of calcium using Small Angle X-ray Scattering (SAXS). Consistent with our prior dynamic light scattering findings for phosphorylated (+P) and non-phosphorylated (−P) LRAP, SAXS analyses revealed radii of gyration (R_g) for LRAP(−P) (46.3 – 48.0 Å) that were larger than those for LRAP(+P) (25.0 – 27.4 Å) at pH 7.4. However, added calcium (up to 2.5 mM) induced significant increases in the R_g of LRAP(+P) (up to 46.4 Å), while it had relatively little effect on LRAP(−P) particle size. Furthermore, SAXS analyses suggested compact folded structures for LRAP(−P) in the presence and absence of calcium, whereas LRAP(+P) conformation changed from an unfolded structure to a more compact structure upon calcium addition. We conclude that the single phosphate group in LRAP(+P) induces functionally important conformational changes, suggesting that phosphorylation may also influence amelogenin conformation and protein-mineral interactions during early stages of amelogenesis.

Keywords

amelogenin; LRAP; phosphorylation; SAXS; conformation

Enamel is the most highly mineralized vertebrate tissue composed of ~96% mineral and 4% organic material and water. During amelogenesis, the ameloblast secretes matrix proteins and is responsible for creating and maintaining an extracellular environment favorable to mineral deposition (1). Amelogenin, the predominant enamel matrix protein, has been shown to undergo self-assembly to form spherical or oblate-shaped nanoparticles (2–4), as

*Corresponding author: Henry C. Margolis, Ph.D., Department of Biomineralization, The Forsyth Institute, 245 First Street, Cambridge Massachusetts 02142, USA, Tel. +1-617-892-8346, Fax: +1-617-892-8432, hmargolis@forsyth.org.

The authors declare that there are no conflicts of interest with respect to this manuscript.

well as elongated structures (5–7), and is believed to play an essential role in guiding the formation of ordered arrays of apatitic crystals during enamel development (5, 8–12). In particular, the N-terminal (containing the only phosphate group on serine-16) and the hydrophilic C-terminal domains of the full-length amelogenin (Fig. 1) have been shown to be critical for proper enamel formation (13–16). It is also believed that during enamel mineral growth, the free calcium ion concentration is regulated, in part, by the binding of calcium to enamel proteins and their proteolytic cleavage products (17–18). The Leucine Rich Amelogenin Peptide (LRAP), a 56 amino-acid alternative splice product of the amelogenin gene found throughout amelogenesis and comprised of the first 33 N-terminal and the last 23 C-terminal amino acids of full-length amelogenin (Fig. 1), has recently been shown by us to share similar behavioral properties with amelogenin with respect to self-assembly and its ability to regulate crystal growth *in vitro* (19–20). As in solution (19), LRAP has been also shown to assemble into nanospheres on fluoroapatite (21) and surfactant-coated gold surfaces (22). Furthermore, it has been shown (23) that non-phosphorylated LRAP and recombinant full-length human amelogenin (rH174) have the same capacity to bind calcium (*i.e.*, 4 – 6 calcium ions per molecule), although the calcium affinity constant for LRAP was greater than that for the full-length amelogenin. Based on similarities of structure and behavior, LRAP has allowed us to investigate the potential role of specific amino-acid domains of amelogenin and phosphorylation in protein self-assembly using Dynamic Light Scattering (DLS) and Transmission Electron Microscopy (TEM). Such studies have illustrated potentially important differences in the self-assembly behavior of phosphorylated and non-phosphorylated LRAP (19). The aim of the present study was to extend these recent findings using Small Angle X-ray Scattering (SAXS), to further investigate the role of phosphorylation in LRAP self-assembly, in the presence and absence of calcium, through comparative studies of phosphorylated (LRAP(+P)) and non-phosphorylated (LRAP(−P)) forms of LRAP (Fig. 1).

Material and methods

Preparation of amelogenin peptides

Phosphorylated LRAP(+P) and non-phosphorylated LRAP(−P) forms of porcine LRAP (56 amino acids) were synthesized commercially (NEO Peptide, Cambridge, MA) and purified as previously described (24). Lyophilized peptides were weighed and dissolved in distilled de-ionized water (DDW) at room temperature to yield stock solutions of 5 – 6 mg/mL. Solutions were kept at room temperature for 30 min and then stored at 4°C for 24h before checking complete dissolution by DLS. Peptide stock solutions were centrifuged (10,900 × g, at 4°C for 20 minutes) just prior to use.

Small Angle X-ray Scattering (SAXS) measurements

Aliquots of peptides were adjusted to pH ~7.4 with small amounts of KOH and HCl to obtain final concentrations of 2 mg/mL (0.31 mM) and 5 mg/mL (0.76 mM) LRAP (total volume 70 μL). In selected experiments, calcium chloride was added to peptide solutions prior to pH adjustment to yield final concentrations of 0.76 mM to 2.5 mM calcium (total volume: 70 μL). Hence, on a molar basis, calcium to protein ratios ranged from 1.0 to 8.1. All sample preparations were carried out at room temperature.

Solution X-ray scattering experiments were carried out at the National Synchrotron Light Source at Brookhaven National Laboratory, on beamline X9 (25). The X-ray wavelength was 0.918 Å and the sample-detector distance was 3.4 m. The sample holder was a 0.9 mm diameter quartz capillary tube open at both ends to allow continuous flow of the sample to avoid X-ray damage. Each measurement required 15 μL of sample and a 30 s exposure time at 13°C. Triplicate measurements were conducted for each experiment. The two-

dimensional images acquired on a PILATUS 300K detector (DECTRIS, Baden, Switzerland) were averaged into one-dimensional scattering curves and then water scattering was subtracted using the pyXS software developed at the beamline. SAXS data were further analyzed using Primus software (26). The data consisted of the scattering vector s (defined as: $s=2\pi/d$ or $4\pi\sin(\theta)/\lambda$) and the corresponding intensity $I(s)$. As noted below in the results section, Guinier and Kratky plots were used to analyze the data. Guinier analyses consisted of the plotting of log I *vs.* s^2 at very low s and were used to determine the radius of gyration R_g and the extrapolated intensity at zero scattering angle I_o, with R_g being the mass distribution of the macromolecule around its center of gravity (27). Kratky analyses were carried out by plotting $I(s)*s^2$ *vs.* s and provided information on peptide folding, as described below (28). The number of molecules per particle was estimated using the following formula: $N = (V_s*N_A*\delta_p)/F_W$; where, $V_S = (4\pi R_g^3)/3$, the density of the protein $\delta_p = 1.44$ g/cm^3 (3), N_A is the Avogadro constant, and $F_W = 6537.52$ Da.

Results

Size of particles formed

SAXS enables the determination of molecular size, shape, and conformational change of a protein molecule in solution. As shown in Fig. 2, the scattering generally exhibited fairly good linear dependence (log $I(s)$ *vs.* s^2) at low s indicating little to no bulk aggregation and allowing further data processing. As shown in Table 1, Guinier plots revealed that the radius of gyration (R_g) was 48.0±0.05 Å for LRAP(−P) and only 25.0±0.50 Å for LRAP(+P) (both at 2 mg/mL, 13° C, pH 7.4), in the absence of added calcium. The R_g values for each peptide were very similar when the peptide concentration was increased to 5 mg/mL, with an R_g of 46.3±0.02 Å for LRAP(−P) and 27.4±0.08 Å for LRAP(+P), under the same experimental conditions. The addition of 2.5 mM calcium to 2 mg/mL solutions of peptide, however, induced a significant increase in the R_g for LRAP(+P) to 43.9±0.05 Å, while it had relatively little effect on the R_g of LRAP(−P), with a value of 46.2±0.03 Å being determined (Table 1). Similar results were obtained for 5 mg/mL peptide solutions containing 2.5 mM calcium with R_g values for LRAP(+P) and LRAP(−P) of 46.4±0.06 Å and 53.9±0.06 Å, respectively. As also shown in Table 1 using peptide concentrations of 5 mg/mL, increasing concentrations of calcium added to LRAP(−P) solutions resulted in a progressive but slight increase in R_g values, whereas increased calcium concentrations resulted in marked concentration-dependent increases in R_g values for LRAP(+P).

Increased I_o values per unit peptide concentration (c), I_o/c (Table 1), calculated for the LRAP(+P) samples, however, were consistent with peptide self assembly (29), as particle sizes (R_g) increased by an overall factor of around two, upon the addition of higher concentrations of calcium. In contrast, as clearly seen in 5 mg/mL samples, a much smaller increase in I_o/c was observed for LRAP(−P) upon calcium addition. Similar increases in the number of molecules per particle were also observed (Table 1). Overall, under comparable conditions, I_o values were larger for LRAP(−P) than for LRAP(+P) and corresponded to a somewhat greater number of molecules per particle.

Determination of conformational changes

Kratky plots ($I(s)*s^2$ *vs.* s) of SAXS data present characteristic and distinctly different shapes for globular folded molecules and extended chain or random coil molecules of similar molecular mass (30–32). Globular macromolecules follow Porod's law and have bell-shaped curves as the clearly defined surface of the protein leads to a drop in intensity with the fourth power of s (31); whereas extended molecules, such as unfolded peptides, lack this peak and have a plateau or increase slightly in the larger s range. As shown in Fig. 3 (A, B and D), the Kratky plot of LRAP(−P) data in the absence of calcium showed a bell-

shaped curve indicating a globular structure. The addition of up to 2.5 mM calcium did not induce an apparent conformational change, as LRAP(−P) exhibited similar bell-shaped curves in the presence of various concentrations of calcium (0.76 mM to 2.5 mM), as it did in its absence (Figs. 3A, 3B and 3D). On the contrary, in the absence of calcium, LRAP(+P) showed a plateau indicating an unfolded extended random structure (Figs. 3A, 3B and 3C). However, a prominent peak appeared upon addition of 2.5 mM calcium ion suggesting the formation of a more globular LRAP(+P)-Ca structure (Figs. 3A and 3B). The extent of folding of the LRAP(+P) peptide was also found to be dependent upon the concentration of calcium added (Fig. 3C). The addition of 0.76 mM calcium induced the formation of a very slight peak, suggesting that the peptide remained mostly in the unfolded state with the appearance of some globular features; upon addition of 1.5 mM calcium the peak appeared more pronounced showing an increase in peptide folding. With the addition of 2.5 mM calcium, the peak of the Kratky plot for LRAP(+P) became even more pronounced and began to resemble that of the non-phosphorylated LRAP(−P) peptide, although the curves remained somewhat distinct at higher values of s (Figs. 3A–D).

Discussion

LRAP, like amelogenin, is a phosphorylated protein that is secreted with a single phosphate group on the serine-16 position (33). Previous studies from our laboratory have shown that this single phosphate group has a major influence on the properties of amelogenin. In particular, in comparison to their non-phosphorylated (recombinant or synthetic) counterparts, phosphorylated (native and synthetic) forms of full-length porcine amelogenin (P173) (7), truncated porcine amelogenin P148 (8), full-length LRAP(+P) (19), and a truncated form of LRAP (LRAP(+P,-CT)) (20) all exhibit the capacity to effectively stabilize amorphous calcium phosphate (ACP) (*i.e.*, preventing its transformation to crystalline hydroxyapatite (HA)), under experimental conditions designed to support the spontaneous formation of calcium phosphates *in vitro.* In sharp contrast to these findings, non-phosphorylated forms of full-length amelogenin and full-length LRAP were shown to guide the formation of ordered bundles of apatitic crystals (5, 8, 19). This latter behavior has been attributed to the ability of full-length amelogenin (6, 7, 15, 34) and LRAP (19) to form higher-order chain-like structures under specified conditions of pH. The presence of calcium has also previously been shown to enhance the formation of chain-like structures of recombinant full-length mouse rM179 (5) and human rH174 (35) amelogenin, and of LRAP (19). Notably, as shown in the latter study, particle sizes and the formation of chain-like structures were enhanced to a greater degree for the phosphorylated form of LRAP. This conclusion was based on DLS and TEM observations. Our present SAXS findings support this conclusion and further demonstrate that the presence of calcium has a profound effect on the size and conformation of phosphorylated LRAP(+P) and little effect on those characteristics of LRAP(−P). This effect is due to the presence of the single phosphate group on serine-16.

Guinier (Table 1) and Kratky (Fig. 3) analyses reveal further assembly and enhanced folding of LRAP(+P) upon the addition of calcium (Figs. 3A, 3B, 3C). Further assembly with added calcium is indicated (Table 1) by marked increases in R_g values, in estimates of the number of molecules per particle, and in I_0/c values. However, it should be noted that I_o values are affected by factors other than particle size (*i.e.,* R_g), such as particle shape and particle density, in the proportion $I_o/c \propto (\rho_{particle} - \rho_{solvent})^2 \times V_{particle}$, where ρ indicates (electron) density and $V_{particle}$ the volume of a single particle (27). Although our present analyses do not take potential differences in these latter factors into consideration, LRAP(+P) and LRAP(−P) were found to behave quite differently in the absence and presence of calcium, particularly with respect to folding. In contrast that seen with LRAP(+P), as was observed previously using circular dichroism (36), the non-phosphorylated form of the peptide

LRAP(−P) does not undergo significant conformational change upon calcium addition (Figs. 3A, 3B, 3D). In addition, as demonstrated here (Fig. 3), LRAP(+P) exhibits a more unfolded structure than LRAP(−P), particularly in the absence and presence of lower concentrations of calcium. It appears that in the presence of calcium, unfolded LRAP(+P) molecules assemble to form more globular-like structures and that the process is primarily triggered by calcium concentration (Table 1 and Fig. 3). As seen in Fig. 3, however, differences in Kratky plots for LRAP(+P) and LRAP(−P) that persist even in the presence of the highest calcium concentration studied at high *s* values, suggest that LRAP(+P) remains somewhat more unfolded than the non-phosphorylated form of LRAP under these conditions. Additional studies will be needed to provide insight into other potential differences in LRAP(+P) and LRAP(−P) self assembly, as briefly noted above.

The remarkable conformational difference between the phosphorylated and non-phosphorylated forms of LRAP shown here offers a possible explanation for the observed differences in assembly behavior and the effects these peptides have on calcium phosphate precipitation *in vitro*. Changes in the folding of LRAP(+P), induced by the addition of calcium, may result from favorable calcium interactions with specific peptide sites that are exposed in the less-folded LRAP(+P) molecules. Such interactions lead to an enhancement of protein-protein interactions and the formation of higher-order anisotropic chain-like structures (19). Hence, based on our present findings, it is concluded that the presence of the single phosphate group in LRAP induces functionally important conformational changes in the protein structure that favor the formation of higher-order protein assemblies. Accordingly, specific structure-changing calcium interactions that take place with LRAP(+P) do not occur with the non-phosphorylated LRAP(−P), since LRAP(−P) is inherently more tightly folded and key calcium binding sites are concealed. Furthermore, observed differences in folding and the tendency for LRAP(+P) to form less folded structures in the absence and presence of calcium may also explain why phosphorylated LRAP(+P) is much more effective in stabilizing ACP nanoparticles and in preventing ACP transformation into HA. The more open structure and the calcium-induced folding of LRAP(+P), in the presence of calcium and phosphate under mineralizing conditions, could lead to a more effective sequestration of forming ACP nanoparticles that prevents ACP transformation to HA. The fact that LRAP(−P) has been shown to only transiently stabilize ACP (19) is consistent with the present findings and this developing hypothesis on the effect of phosphorylation on protein conformation and mineralization. However, it is important to consider that previous findings also show that LRAP(−P) (19), like full-length non-phosphorylated amelogenins rM179 (5) and rP172 (8), have the capacity to regulate the formation of ordered arrays of apatitic crystals by guiding the alignment, fusion and subsequent transformation of initially formed ACP nanoparticles (8). This capability was found to depend on the presence of the hydrophilic C-terminus in both amelogenin and LRAP (20). Based on these collective findings, additional processes (*e.g.,* proteolysis or de-phosphorylation, as we have recently discussed (19)) may be involved *in vivo* to trigger the subsequent transformation of initially formed ACP particles, as found in early stages of developing enamel (37). We propose that initially formed ACP mineral in developing enamel is stabilized by native phosphorylated amelogenins that guide the accumulation and linear arrangement of amorphous nano-particles that serve as precursors to enamel crytallites.

In conclusion, we have shown that the single phosphate group in LRAP(+P) induces functionally important conformational changes, particularly with respect to calcium interactions. Although further studies are needed, the present findings suggest that phosphorylation may also influence amelogenin conformation and subsequent protein-mineral interactions during early stages of amelogenesis.

Acknowledgments

This work was supported by grant DE-016376 (H.C.M) from the National Institute of Dental and Craniofacial Research. Use of beamline X9 and the National Synchrotron Light Source, Brookhaven National Laboratory, was supported by the U.S. Department of Energy, Office of Science, Office of Basic Energy Sciences, under Contract No. DE-AC02-98CH10886.

References

1. Nanci, A. Enamel: composition, formation and structure. In: NANCI. , editor. Ten Cate's oral histology - development, structure, and function. 7th edn.. St. Louis: Mosby Inc.; 2008. p. 141-190.
2. Aichmayer B, Margolis HC, Sigel R, Yamakoshi Y, Simmer JP, Fratzl P. The onset of amelogenin nanosphere aggregation studied by small-angle X-ray scattering and dynamic light scattering. J Struct Biol. 2005; 151:239–249. [PubMed: 16125972]
3. Aichmayer B, Wiedemann-Bidlack FB, Gilow C, Simmer JP, Yamakoshi Y, Emmerling F, Margolis HC, Fratzl P. Amelogenin nanoparticles in suspension: Deviations from spherical shape and pH-dependent aggregation. Biomacromolecules. 2010; 11:369–376. [PubMed: 20038137]
4. Fincham AG, Moradian-Oldak J, Diekwisch TGH, Lyaruu DM, Wright JT, Bringas JRP, Slavkin HC. Evidence for amelogenin "nanospheres" as functional components of secretory-stage enamel matrix. J Struct Biol. 1995; 115:50–59. [PubMed: 7577231]
5. Beniash E, Simmer JP, Margolis HC. The effect of recombinant mouse amelogenins on the formation and organization of hydroxyapatite crystals in vitro. J Struct Biol. 2005; 149:182–190. [PubMed: 15681234]
6. Wiedemann-Bidlack FB, Beniash E, Yamakoshi Y, Simmer JP, Margolis HC. pH triggered self-assembly of native and recombinant amelogenins under physiological pH and temperature in vitro. J Struct Biol. 2007; 160:57–69. [PubMed: 17719243]
7. Wiedemann-Bidlack FB, Kwak SY, Beniash E, Yamakoshi Y, Simmer JP, Margolis HC. Effects of phosphorylation on the self-assembly of native full-length porcine amelogenin and its regulation of calcium phosphate formation in vitro. J Struct Biol. 2011; 173:250–260. [PubMed: 21074619]
8. Kwak SY, Wiedemann-Bidlack FB, Beniash E, Yamakoshi Y, Simmer JP, Litman A, Margolis HC. Role of 20-kDa amelogenin (P148) phosphorylation in calcium phosphate formation in vitro. J Biol Chem. 2009; 284:18972–18979. [PubMed: 19443653]
9. Margolis HC, Beniash E, Fowler CE. Role of macromolecular assembly of enamel matrix proteins in enamel formation. J Dent Res. 2006; 85:775–793. [PubMed: 16931858]
10. Moradian-Oldak J, Tan J, Fincham AG. Interaction of amelogenin with hydroxyapatite crystals: an adherence effect through amelogenin molecular self-association. Biopolymers. 1998; 46:225–238. [PubMed: 9715666]
11. Tarasevich BJ, Howard CJ, Larson JL, Snead ML, Simmer JP, Paine M, Shaw WJ. The nucleation and growth of calcium phosphate by amelogenin. J Cryst Growth. 2007; 304:407–415.
12. Wang L, Guan X, Du C, Moradian-Oldak J, Nancollas GH. Amelogenin promotes the formation of elongated apatite microstructures in a controlled crystallization system. J Phys Chem C. 2007; 111:6398–6404.
13. Paine ML, Snead ML. Protein interactions during assembly of the enamel organic extracellular matrix. J Bone Miner Res. 1997; 12:221–227. [PubMed: 9041053]
14. Paine ML, Luo W, Zhu DH, Bringas JRP, Snead ML. Functional Domains for Amelogenin revealed by compound genetic defects. J Bone Miner Res. 2003; 18:466–472. [PubMed: 12619931]
15. Paine ML, Wang HJ, Snead ML. Amelogenin self-assembly and the role of the proline located within the carboxyl-teleopeptide. Connect Tissue Res. 2003; 44(Suppl 1):52–57. [PubMed: 12952174]
16. Pugach MK, Li Y, Suggs C, Wright JT, Aragon MA, Yuan ZA, Simmons D, Kulkarni AB, Gibson CW. The amelogenin C-terminus is required for enamel development. J Dent Res. 2010; 89:165–169. [PubMed: 20042744]

17. Yamakoshi Y, Tanabe T, Oida S, Hu CC, Simmer JP, Fukae M. Calcium binding of enamel proteins and their derivatives with emphasis on the calcium-binding domain of porcine sheathlin. Arch Oral Biol. 2001; 46:1005–1014. [PubMed: 11543707]
18. Aoba T, Moreno EC. The enamel fluid in the early secretory stage of porcine amelogenesis: chemical composition and saturation with respect to enamel mineral. Calcif Tissue Int. 1987; 41:86–94. [PubMed: 3115550]
19. Le Norcy E, Kwak SY, Wiedemann-Bidlack FB, Beniash E, Yamakoshi Y, Simmer JP, Margolis HC. Leucine-rich amelogenin peptides regulate mineralization *in vitro* . J Dent Res. 2011; 90:1091–1097. [PubMed: 21653221]
20. Le Norcy E, Kwak SY, Wiedemann-Bidlack FB, Beniash E, Yamakoshi Y, Simmer JP, Margolis HC. Potential role of the amelogenin N-terminus in the regulation of calcium phosphate formation in vitro. Cells Tissues Organs. 2011; 194:188–193. [PubMed: 21576914]
21. Habelitz S, Denbesten PK, Marshall SJ, Marshall GW, Li W. Self-assembly and effect on crystal growth of the leucine-rich amelogenin peptide. Eur J Oral Sci. 2006; 114(Suppl 1):315–319. [PubMed: 16674705]
22. Tarasevich BJ, Lea S, Shaw WJ. The leucine rich amelogenin protein (LRAP) adsorbs as monomers or dimers onto surfaces. J Struct Biol. 2010; 169:266–276. [PubMed: 19850130]
23. Le TQ, Gochin M, Featherstone JD, Li W, Denbesten PK. Comparative calcium binding of leucine-rich amelogenin peptide and full-length amelogenin. Eur J Oral Sci. 2006; 114(Suppl 1): 320–326. [PubMed: 16674706]
24. Nagano T, Kakegawa A, Yamakoshi Y, Tsuchiya S, Hu JC, Gomi K, Arai T, Bartlett JD, Simmer JP. Mmp-20 and Klk4 cleavage site preferences for amelogenin sequences. J Dent Res. 2009; 88:823–828. [PubMed: 19767579]
25. Allaire M, Yang L. Biomolecular solution X-ray scattering at the National Synchrotron Light Source. J Synchrotron Radiat. 2011; 18:41–44. [PubMed: 21169689]
26. Konarev PV, Volkov VV, Sokolova AV, Koch MHJ, Svergun DI. PRIMUS: a Windows PC-based system for small-angle scattering data analysis. J Appl Cryst. 2003; 36:1277–1282.
27. Guinier, A.; Fournet, G. Small-Angle Scattering of X-rays. New York: Wiley; 1955.
28. Glatter, O.; Kratky, O., editors. Small-angle X-ray Scattering. London: Academic Press; 1982.
29. Kearney KR, Moore PB. X-ray solution-scattering studies of active and inactive Escherichia coli ribosomal subunits. J Mol Biol. 1983; 170:381–402. [PubMed: 6355486]
30. Semisotnov GV, Kihara H, Kotova NV, Kimura K, Amemiya Y, Wakabayashi K, Serdyuk IN, Timchenko AA, Chiba K, Nikaido K, Ikura T, Kuwajima K. Protein globularization during folding. A study by synchrotron small-angle X-ray scattering. J Mol Biol. 1996; 262:559–574. [PubMed: 8893863]
31. Doniach S. Changes in biomolecular conformation seen by small angle X-ray scattering. Chem Rev. 2001; 101:1763–1778. [PubMed: 11709998]
32. Putnam CD, Hammel M, Hura GL, Tainer JA. X-ray solution scattering (SAXS) combined with crystallography and computation: defining accurate macromolecular structures, conformations and assemblies in solution. Q Rev Biophys. 2007; 40:191–285. [PubMed: 18078545]
33. Fincham AG, Moradian-Oldak J, Sarte PE. Mass-spectrographic analysis of a porcine amelogenin identifies a single phosphorylated locus. Calcif Tissue Int. 1994; 55:398–400. [PubMed: 7866922]
34. Buchko GW, Tarasevich BJ, Bekhazi J, Snead ML, Shaw WJ. A solution NMR investigation into the early events of amelogenin nanosphere self-assembly initiated with sodium chloride or calcium chloride. Biochemistry. 2008; 47:13215–13222. [PubMed: 19086270]
35. He X, Wu S, Martinez-Avila O, Cheng Y, Habelitz S. Self-aligning amelogenin nanoribbons in oil-water system. J Struct Biol. 2011; 174:203–212. [PubMed: 21134461]
36. Shaw WJ, Ferris K. Structure, orientation, and dynamics of the C-terminal hexapeptide of LRAP determined using solid-state NMR. J Phys Chem B. 2008; 112:16975–16981. [PubMed: 19368031]
37. Beniash E, Metzler RA, Lam RSK, Gilbert Pupa. Transient amorphous calcium phosphate in forming enamel. J Struct Biol. 2009; 166:133–143. [PubMed: 19217943]

P173: **MPLPPHPGHPGYINF*S*^{P}YEVLTPLKWYQNMIRHP**YTSYGYEPMGGWLHHQIIPVVSQQT
PQSHALQPHHIPMVPAQQPGIPQQPMMPLPGQHSMTPTQHHQPNLPLPAQQPFQPQP
VQPQPHQPLQPQSPMHPIQPLLPQPPLPPLPPMFSMQ**SLLPDLPLEAWPATDKTKREEVD**
hydrophilic domain

LRAP(+P): MPLPPHPGHPGYINF***S***^{P}YEVLTPLKWYQNMIRHPSLLPDLPLEAWPATDKTKREEVD

LRAP(-P): MPLPPHPGHPGYINF***S***YEVLTPLKWYQNMIRHPSLLPDLPLEAWPATDKTKREEVD

Figure 1. Amino-acid sequences of the full-length porcine amelogenin (P173) and the phosphorylated (+P) and non-phosphorylated (−P) LRAP peptides

Note that LRAP is composed exclusively of the N- and C-terminal domains (shown in bold type) of the full-length molecule.

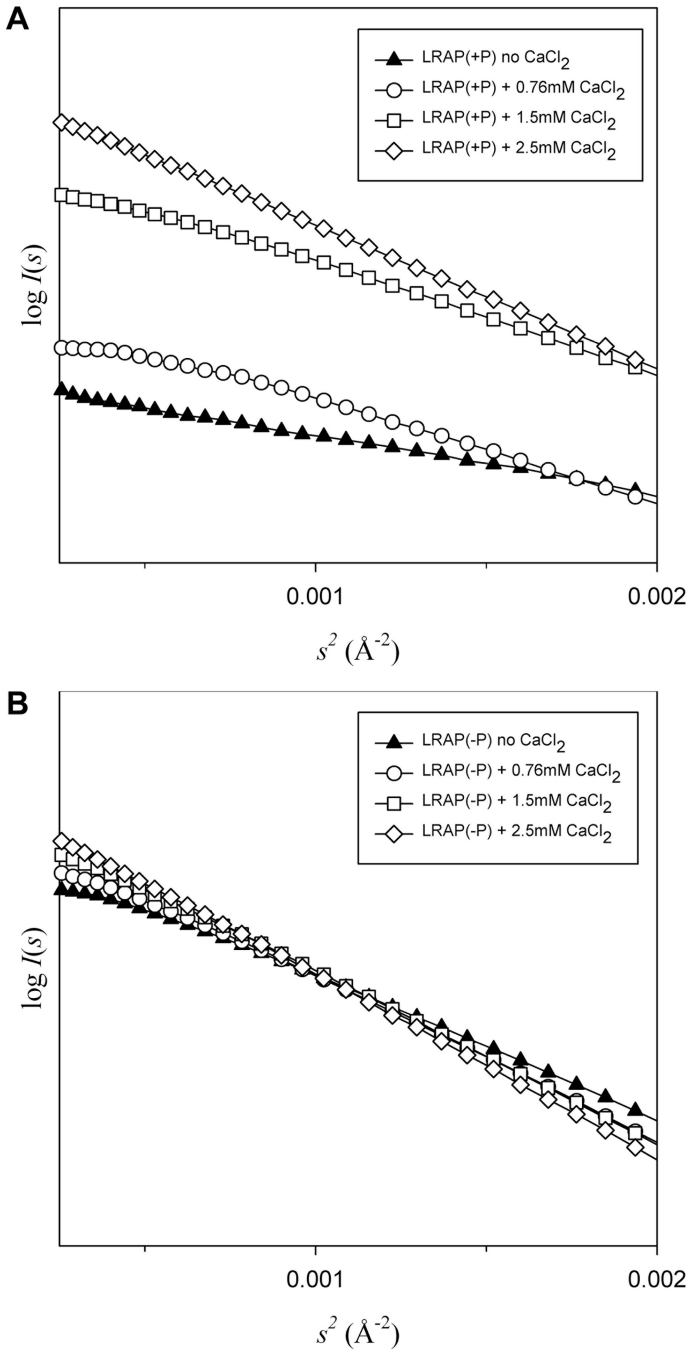

Figure 2.

The Guinier region of the scattering curve for LRAP(+P) (A) and LRAP(−P) (B) data recorded in the absence and in the presence of 0.76mM to 2.5 mM calcium chloride ($CaCl_2$). Curves in (A) and (B) exhibit fairly good linear dependence of log $I(s)$ *vs.* s^2 indicating little to no bulk aggregation. Data shown are for 5 mg/mL peptide concentrations.

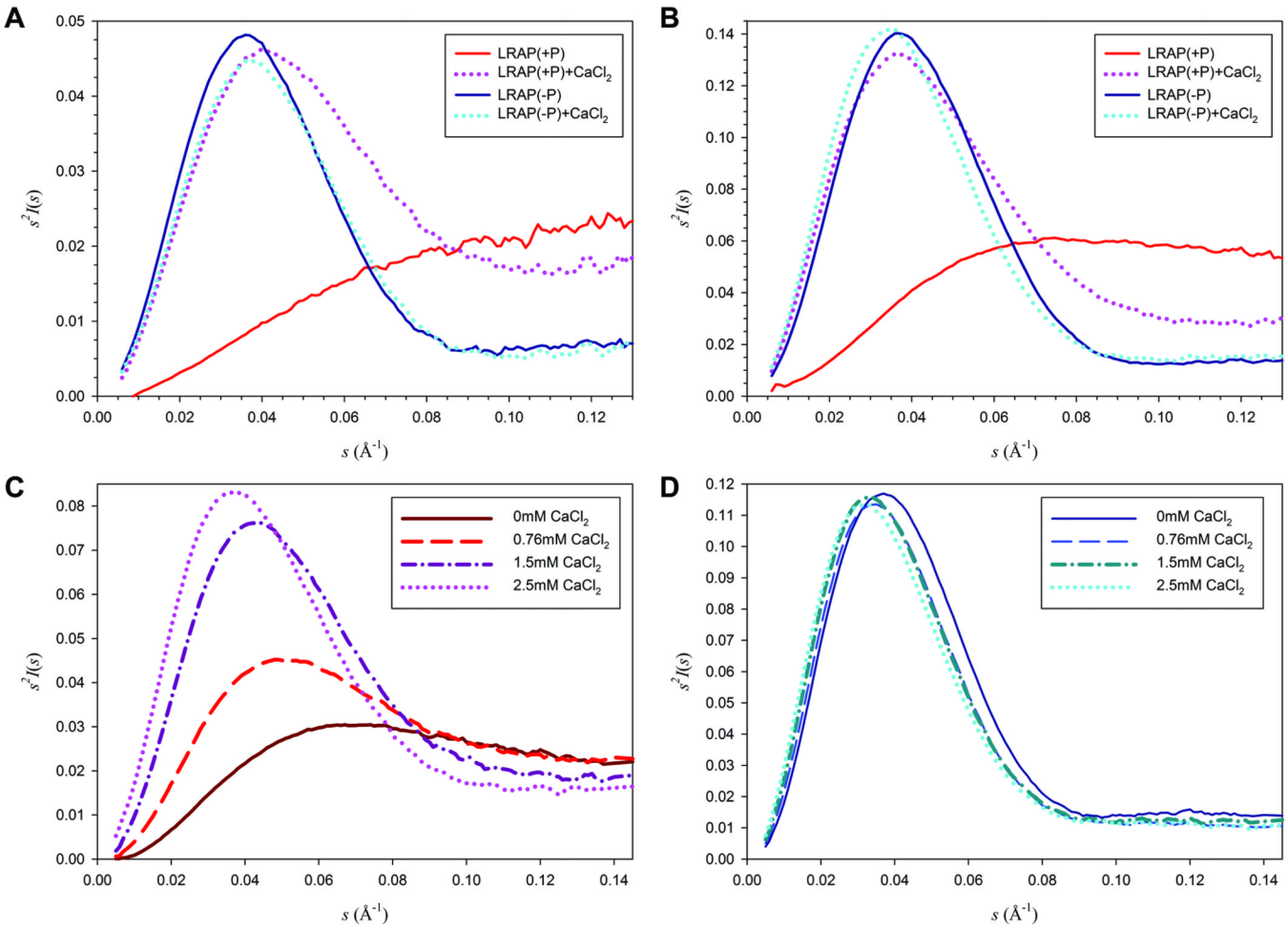

Figure 3. SAXS Analyses of LRAP(−P) and LRAP(+P)

Kratky plots of LRAP(−P) and LRAP(+P) at 2 mg/mL (A) and 5 mg/mL (B ,C and D) were determined in the absence and in the presence of 2.5 mM $CaCl_2$ (A and B) and from 0 to 2.5 mM $CaCl_2$ (C and D). The plots of LRAP(−P) in the absence and presence of calcium showed a similar bell-shaped curve indicating globular structures (A, B and D). However, in the absence of calcium (A and B), LRAP(+P) showed a plateau indicating an unfolded structure, whereas a prominent peak appeared upon addition of 2.5 mM calcium (A and B). This latter peak was found to become increasingly more pronounced as a function of calcium concentration (C), suggesting the formation of a more globular LRAP(+P) structure in the presence of added calcium.

Table 1

Guinier analyses of effect of peptide and calcium concentrations on particle size.

		Guinier				
Peptide concentration	**[$CaCl_2$] (mM)**	**R_g (Å)**	**Error**	**I_o**	**I_o/c**	**Number of molecules per particle**
2mg/ml						
LRAP(+P)	0	25.0	0.489	8.39	4.2	9
	2.5	43.9	5.34E-02	73.12	36.6	47
LRAP(−P)	0	48.0	5.34E-02	100.33	50.2	61
	2.5	46.2	2.59E-02	85.87	42.9	55
5mg/ml						
	0	27.4	7.77E-02	20.304	4.06	11
LRAP(+P)	0.76	35.5	5.32E-02	51.829	10.4	25
	1.5	40.7	4.08E-02	115.14	23.0	37
	2.5	46.4	6.41E-02	165.03	33.0	56
	0	46.3	2.20E-02	230.17	46.0	55
LRAP(−P)	0.76	49.5	2.80E-02	254.58	50.9	67
	1.5	52.0	4.30E-02	286.57	57.3	78
	2.5	53.9	6.24E-02	302.99	60.6	87

LRAP(−P) and LRAP(+P) exhibit similar radii of gyration (R_g) at 2 and 5 mg/mL. The R_g of LRAP(+P) is half of that of LRAP(−P) in the absence of calcium at pH~7.4. R_g and *I*o/c for LRAP(−P) increased slightly upon addition of up to 2.5 mM calcium, whereas marked and progressive increases in these parameters are observed in the presence of LRAP(+P), upon the addition calcium. I_O is the extrapolated intensity at zero scattering angle and *Io/c* represents the I_O values per unit peptide concentration. The estimated number of molecules calculated from the R_g is presented for comparison purposes.